Available online at www.sciencedirect.com
SCIENCE DIRECT®
Journal of Sound and Vibration 280 (2005) 997–1015
JOURNAL OF SOUND AND VIBRATION
www.elsevier.com/locate/jsvi

An analytical study of the effect of process damping on reamer vibrations

David N. Dilley[a,*], Phil V. Bayly[a], Brian T. Whitehead[b], Sean G. Calvert[c]

[a]*Mechanical Engineering, Washington University, Box 1185, St. Louis, MO 63130, USA*
[b]*Boeing Military Aircraft and Missile Systems, P.O. Box 516, St. Louis, MO 63166, USA*
[c]*Blue Road Research, Inc. 2555 N.E. 205th Avenue, Troutdale, OR 97060, USA*

Received 9 September 2003; accepted 5 January 2004
Available online 5 November 2004

Abstract

A frequency-domain approach is used to study the effects of a velocity-dependent force caused by the rubbing between the reamer margins and the hole wall. The solution method determines tool stability and hole form. The velocity-dependent force, colloquially known as process damping, has been used in turning and milling, where it has been shown to stabilize the system at low spindle speeds. The addition of the process-damping model in the reamer model stabilizes self-excited chatter near the first fundamental tool bending frequency, but destabilizes low-frequency vibration. The method yields combinations of cutting speed and depth of cut that bind stable cutting regions. The boundaries for reaming with no process damping closely resemble the shape of milling stability diagrams, but the small radial depth of cut is unrealistic. The addition of process damping changes the shape of the stability regions and also increases the stable depth of cut. Notably, eigenvalue solutions are found with increased process damping that lead to low-frequency whirling modes, which resemble those found in practice. A simulation using a numerical Euler integration technique will be used to match the analytical model. The simulation will allow for future research using nonlinear models, uneven tooth spacing, and arbitrary initial hole profile data.

*Corresponding author. Current address: D3 Vibrations Inc., 220 S. Main, Royal Oak, MI 48067, USA. Tel. +1-248-2597808; fax: +1-248-5419942.
E-mail address: d3v@sbcglobal.net (D.N. Dilley).

0022-460X/$ - see front matter © 2004 Published by Elsevier Ltd.
doi:10.1016/j.jsv.2004.01.054

Nomenclature

ξ, η	tool-fixed frame on cutting tooth geometry (m)
Ξ, H	tool-fixed frame in uncoupled structural directions (m)
x, y	lab-fixed frame (m)
$\mathbf{T}$	transformation matrix
z	axial, or feed, direction (m)
θ	angle between ξ-axis and x-axis (rad)
ϑ	angle between ξ-axis and Ξ-axis (rad)
Ω	spindle speed (rad/s), equals $\dot{\theta}$
t	time (s)
N_t	number of teeth
τ_{0i}	time delay between each tooth pass (s)
τ_0	time delay between each tooth pass for equally spaced tools (s)
τ	discrete time delay between each tooth pass for equally spaced tools (steps)
ϕ_i	tooth position from ξ-axis (rad)
$\Delta\phi_i$	tooth spacing between each tooth (rad)
k_s	cutting pressure coefficient ($\mathrm{N/m^2}$)
α	cutting force angle (rad)
k_r	rubbing stiffness coefficient (N/rad)
r_0	mean tool radius (m)
R_{00}	pilot hole radius (m)
ρ	chamfer angle (radians)
H_{nom}	mean feed per tooth (m)
L_{nom}	mean chip length in 2D frame (m)
ΔL	dynamic uncut chip length (m)
μ_r	geometry ratio
μ	regeneration factor
μ_f	coefficient of friction
ω_n	tool natural frequency (rad/s)
m_{ii}	tool modal mass in *ii* direction (N/m)
k_{ii}	tool stiffness in *ii* direction (N/m)
c_{ii}	tool damping in *ii* direction (N s/m)
ζ_{ii}	tool damping ratio in *ii* direction
$\mathbf{M}$	mass matrix (kg)
$\mathbf{C}_r$	damping matrix, rotating coordinate system (N s/m)
$\mathbf{K}_r$	stiffness matrix, rotating coordinate system (N/m)
$\mathbf{K}_{cc}$	cutting pressure matrix, rotating coordinate system ($\mathrm{N/m^2}$)
$\mathbf{C}_{pd}$	process damping matrix, rotating coordinate system (N s/m)
$\mathbf{G}_{pd}(\omega, \Omega)$	FRF for system in rotating frame (m/N)
$\mathbf{R}(\omega, \Omega)$	regeneration matrix ($\mathrm{N/m^2}$)
$\mathbf{P}_{pd}(\omega, \Omega)$	stability matrix, rotating coordinate system ($\mathrm{m^{-1}}$)
$\vec{F}_{\mathrm{ext}}$	external force vector (N)
$\vec{F}_c$	cutting force vector (N)
$\vec{F}_r$	process damping force vector (N)
n	discrete step
$\mathrm{d}t$	discrete time step
$\Delta\omega$	frequency interval for numerical search of zero-axis crossing

1. Introduction

Reaming is a common metal-cutting process, and the quality of hole form is often a critical issue. Stability and hole form in precision holemaking is of interest because of reduction in rework cost and part fatigue issues. An understanding of tool vibration during cutting, and the resultant effects on hole form, is an important step toward achieving high-precision holes. Tool dynamics was originally studied in turning and endmilling processes where time-delayed regenerative forces were responsible for instability [1–3]. These authors predicted stability regions using frequency-domain analysis where combinations of axial depth of cut (ADOC) and spindle speed (rpm) provided high metal removal rates. Later, more sophisticated analytical methods were used to predict endmill stability lobes with greater accuracy [4,5].

The use of stability diagrams for milling has had a significant influence on industry in recent years, but dynamic studies in drilling, reaming, and boring have had less impact. Fujii, Marui, and Ema studied out of round, or lobed holes, in drilling by showing how tool whirling affects final hole form [6–8]. In experimental investigations of reaming, Sakuma and Kiyota [9,10] have shown that motion at N_t cycle/rev, where N_t is the number of cutting flutes, leads to lobed holes with $N_t - 1$ or $N_t + 1$ lobes. Li et al. [11] studied the effect of rotation in boring bars. The formation of lobed holes in reaming was analyzed quasi-statically by Bayly et al. [12], and stability boundaries in drilling and reaming with no process damping have been estimated by Metzler et al. [13] using a method similar to Altintas and Budak [5].

In practice, two types of instability can be distinguished: (1) regenerative chatter (vibration of the tool near its natural frequency) and (2) low-frequency whirling vibrations leading to out-of-round holes, as shown in Fig. 1. The lobed or multi-pointed holes that result from the latter instability can appear to be within specification when measuring opposite points, yet may still fail to accept a round fastener of the appropriate size.

This work extends the analysis by Metzler et al. [13] of a dynamic model of reaming by showing the effect of process damping on the stability regions. Unlike milling and turning, which are simply stabilized by process damping, low-frequency modes responsible for lobed holes in reaming are destabilized from the interaction of process damping with cutting and bending forces on the rotating tool.

2. Analytical model

2.1. Tool dynamics

In use, a straight-fluted reamer typically exhibits bending vibration with minimal torsional or axial vibration. This simplifies the analysis by modeling only the primary bending modes. Small linear displacements are assumed since the movement at the tool tip is minimal compared to the tool length. In addition, slender tools are typically modeled using the first bending mode, as the higher modes are much stiffer and have less influence on hole form, especially with forcing frequencies less than the natural frequency of the first bending mode. These assumptions allow the reamer to be modeled as a two-degree-of-freedom (2dof) lumped parameter system at the tool tip with an uncoupled single mode in each direction, while the external forces act as a single point load on the tool.

There are three reference frames that will be used in this paper, as shown in Fig. 2. The lab-fixed frame, x–y, is a non-rotating frame. The tool-fixed frame with respect to the cutting teeth, ξ–η, is used for cutting forces, while a tool-fixed frame, Ξ–H, with respect to the uncoupled directions is used for developing the structural model. A symmetric tool with four flutes is virtually uncoupled; so $\xi - \eta \approx \Xi - H$. However, a tool with six flutes requires a rotation angle, ϑ, between the tool-fixed frames. An equivalent modal mass is assumed suspended by springs and dampers in the Ξ–H frame, where parameter values can be identified from experimental modal tests of the tool. The dynamic parameters (m, c, k) can be different for each direction; however, they will be considered identical in this qualitative study of a symmetric reamer. The type of model used depends on the structure. If the non-rotating portion of the machine tool dominates the dynamics, a fixed system

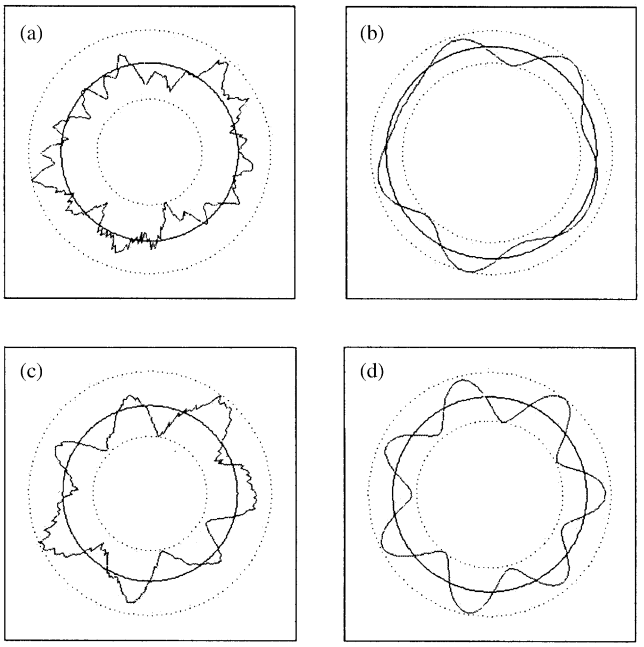

Fig. 1. A typical hole profile for a reamer showing observations of lobing. Reaming was performed at 500 rpm, 12.7 mm tool diameter, 11.9 mm pilot hole (radial depth of cut = 0.4 mm). (a) Hole profile, feed = 0.15 mm/rev, from a roundness and concentricity measuring machine (Talyrond T130 (Taylor and Hobson, UK). This hole has a roundness error of 19 μm. Panel (b) shows the hole profile after filtering out frequencies above 8/rev. It looks like a 5-lobed hole. However the high frequency may have created the long flat areas on a 7-lobed hole. (c) Hole profile, feed = 0.30 mm/rev, from Talyrond. This predominantly 7-lobed hole has roundness error of 20 μm. Panel (d) shows the hole profile after filtering out frequencies above 8/rev. Roundness error was calculated by least-squares fitting a circle to the hole profile and calculating the difference between the diameters of the concentric circles tangent to the maximum and minimum deviations.

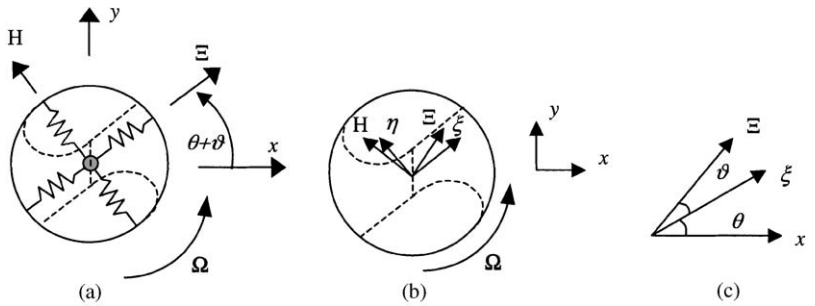

Fig. 2. Reference frames and angles for 2dof tool model: x–y is lab fixed; ξ–η tool fixed on the main cutting edge; Ξ–H tool fixed on the structural eigenvalues. (a) Structural diagram, (b) force diagram, (c) transformation angles.

is recommended. If the rotating portion (spindle arbor, toolholder and tool geometry) dominates the dynamics, a rotating system is suggested. As shown by Metzler et al. [13] a fixed frame is identical to a rotating frame model for symmetric tools with three or more teeth.

Since the derivation of the cutting and rubbing forces in the fixed frame can lead to time-varying coefficients for asymmetric tools, this difficulty is avoided when using a coordinate frame that rotates with the tool. Therefore, the cutting and process damping forces will be modeled in the ξ–η frame. The transformation matrix between the frames is

$$\vec{\xi} = \begin{bmatrix} \xi \\ \eta \end{bmatrix} = \left(\begin{bmatrix} \cos\theta & \sin\theta \\ -\sin\theta & \cos\theta \end{bmatrix} \right) \begin{bmatrix} x \\ y \end{bmatrix} = \mathbf{T}(\theta)\vec{x},$$
$$\vec{\Xi} = \begin{bmatrix} \Xi \\ \mathrm{H} \end{bmatrix} = \left(\begin{bmatrix} \cos\vartheta & \sin\vartheta \\ -\sin\vartheta & \cos\vartheta \end{bmatrix} \right) \begin{bmatrix} \xi \\ \eta \end{bmatrix} = \mathbf{T}(\vartheta)\vec{\xi}. \tag{1}$$

The rotating system includes centripetal and Coriolis coupling terms in the dynamic matrices [11,13] that are dependent on the spindle rotational speed, Ω, in radians per second

$$\mathbf{M} \begin{bmatrix} \ddot{\Xi} \\ \ddot{\mathrm{H}} \end{bmatrix} + \mathbf{C}_r \begin{bmatrix} \dot{\Xi} \\ \dot{\mathrm{H}} \end{bmatrix} + \mathbf{K}_r \begin{bmatrix} \Xi \\ \mathrm{H} \end{bmatrix} = \vec{F}_{\mathrm{ext}}, \tag{2}$$

where

$$\mathbf{M} = \begin{bmatrix} m_{\Xi\Xi} & 0 \\ 0 & m_{HH} \end{bmatrix}, \quad \mathbf{C}_r = \begin{bmatrix} c_{\Xi\Xi} & -2m_{\Xi\Xi}\Omega \\ 2m_{HH}\Omega & c_{HH} \end{bmatrix}, \quad \mathbf{K}_r \begin{bmatrix} k_{\Xi\Xi} - m_{\Xi\Xi}\Omega^2 & -c_{\Xi\Xi}\Omega - m_{\Xi\Xi}\dot{\Omega} \\ c_{HH}\Omega - m_{HH}\dot{\Omega} & k_{HH} - m_{HH}\Omega^2 \end{bmatrix}$$

and the external forces include cutting and rubbing forces in the rotating frame

$$\vec{F}_{\mathrm{ext}} = \vec{F}_c + \vec{F}_r. \tag{3}$$

In most cases, the angular acceleration, $\dot{\Omega}$, will equal zero as most spindles rotate at a constant rpm. Again, it remains in the equation for generality. Since the forcing function is modeled in the rotating frame, the centripetal and Coriolis terms are necessary for the rotating tool model. The stability analysis for a symmetric four-flute reamer, Fig. 3, shows that removing the centripetal and Coriolis terms greatly affects the stability regions. Remember, the rotating forcing function was used. So this does not show the difference between a fixed and rotating model, only the effect of removing the coupling terms.

2.2. Cutting forces

Dynamic cutting forces are taken as the result of deviations of the uncut chip thickness, ΔL, from the nominal value. As shown in Fig. 4 for a four-fluted reamer, the displacement of the reamer $\vec{\xi} = [\xi\ \eta]^{\mathrm{T}}$ affects ΔL on each tooth, resulting in a net force. A deflection at the time of the previous tooth passage, $\vec{\xi}(t - \tau_0)$ where τ_0 is the time between successive tooth passes for even spaced tools, also changes the uncut chip thickness. This delay term is classically referred to as regeneration. It is shown in Fig. 5 that tool displacement increases the uncut chip area by adding

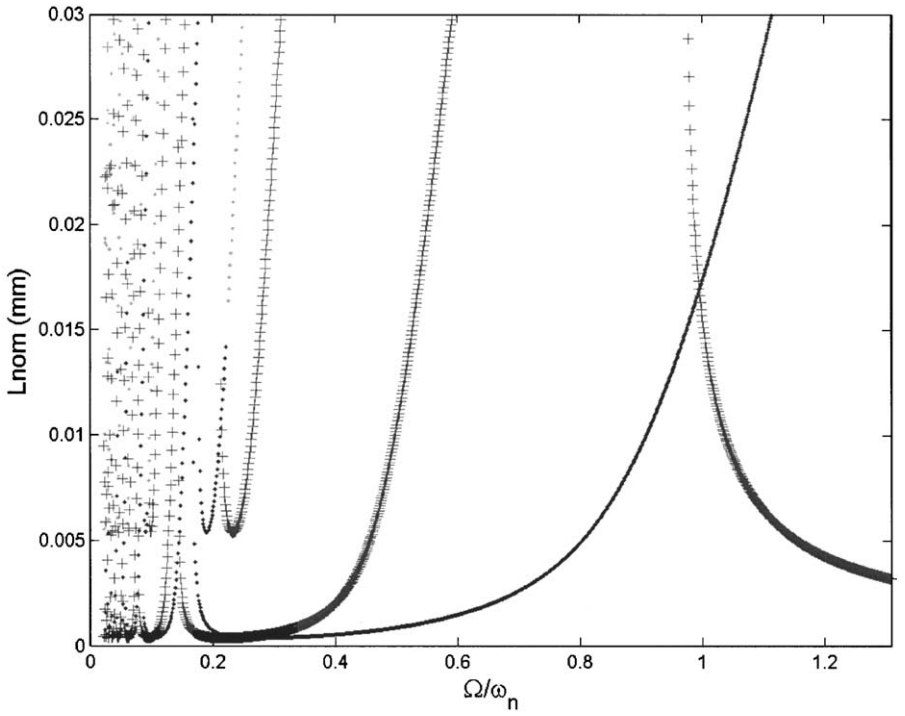

Fig. 3. Effect of centripetal and Coriolis terms in a stability analysis for a four-flute symmetric reamer: $\omega_\pi = 382\,\text{Hz}$, $k = 186,000\,\text{N/m}$, $\zeta = 0.002$, no process damping. The plots shown by '.' include these terms and '+' are the results of the terms equal zero. The non-dimensional value Ω/ω_n equal one when spindle speed is 22,920 rpm.

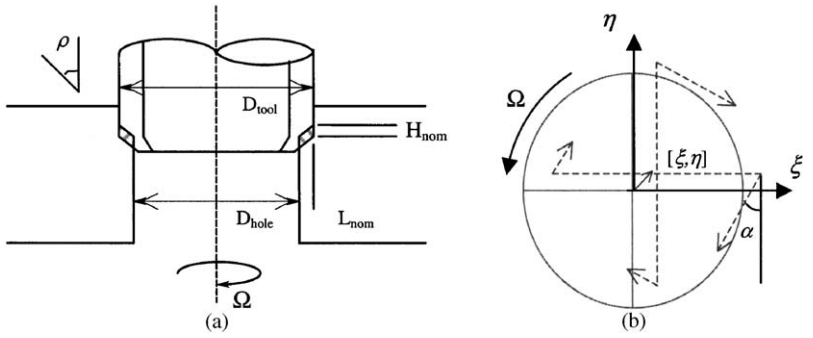

Fig. 4. (a) Nominal chip thickness, (b) change in chip thickness due to tool displacement (α = cutting force angle).

material on the side and also in the z-direction. These will be referred to as side and up–down regeneration, respectively.

The solution method shown in a later section is simplified if a single stability variable is used; therefore, this model will use the nominal radial length of cut (L_{nom}) as the stability variable, where L_{nom} is also known as the radial depth of cut (RDOC) for a straight-fluted reamer. The feed rate affects stability, but only one stability variable is desired, so the feed per tooth (H_{nom}) will be

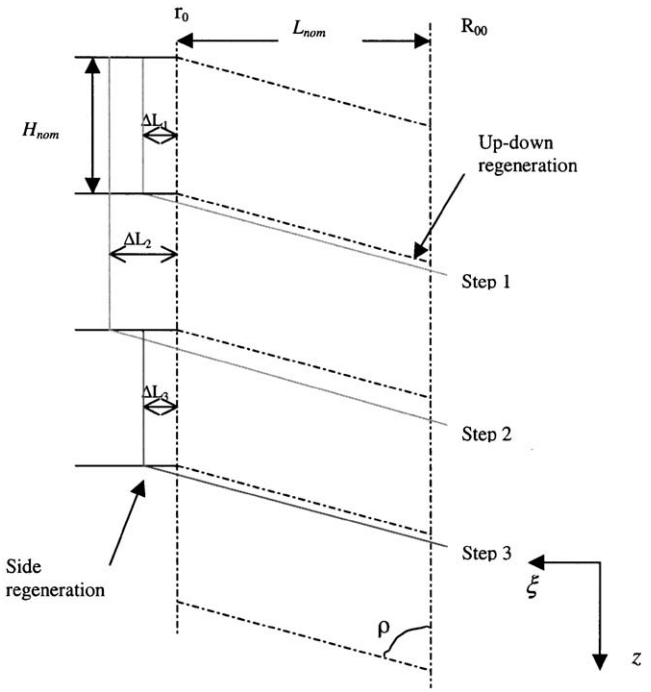

Fig. 5. Uncut chip area for a straight-fluted reamer at one position of the hole. Four tooth passes are shown.

scaled as a ratio of L_{nom}, Eq. (4). This assumption is reasonable since many reamer processes are designed with the feed per tooth as a ratio of the radial depth of cut, as the nominal chip area is H_{nom} multiplied by L_{nom}:

$$\mu_r = \frac{H_{\text{nom}}}{L_{\text{nom}}}. \tag{4}$$

The amount of material left to cut from the previous pass will be found by multiplying the regeneration factor, μ, by the tool displacement from the previous pass. The regeneration factor is dependent on the Chamfer angle (ρ), H_{nom}, and L_{nom}. In this model, for simplicity any cutting on the flutes above the tip is neglected. The vast majority of material is removed at the tool tip, and we hypothesize that the dominant effects above the tip are burnishing and elastic deformation as the tool traces its initial profile. A numerical simulation, such as a finite element method or an Euler simulation shown in Section 5, would be required to solve a more detailed model including forces from additional tooth passes, elasticity, and plasticity from burnishing for improved quantitative prediction capability:

$$\mu = \frac{\mu_r + 1/\tan\rho}{2\mu_r + 1/\tan\rho}. \tag{5}$$

Since μ is always less than one, the solution is nontrivial as will be shown later in the stability analysis. The force vector with respect to the rotating frame for a symmetric reamer is found by

summing the force on each tooth

$$\begin{bmatrix} F_{c\xi} \\ F_{c\eta} \end{bmatrix} = L_{\text{nom}}\left(2\mu_r + \frac{1}{\tan\,\rho}\right)k_s \sum_{i=1}^{N_t} \begin{bmatrix} c_i C_i & s_i C_i \\ c_i S_i & s_i S_i \end{bmatrix} \left(\mathbf{I}\begin{bmatrix} \xi(t) \\ \eta(t) \end{bmatrix} - \mu\mathbf{T}(\Delta\phi_i)\begin{bmatrix} \xi(t-\tau_{0i}) \\ \eta(t-\tau_{0i}) \end{bmatrix}\right), \tag{6}$$

where

$$c_i = \cos(\phi_i), \quad s_i = \sin(\phi_i), \quad C_i = \cos(\phi_i - \pi/2 - \alpha), \quad S_i = \sin(\phi_i - \pi/2 - \alpha),$$

where ϕ_i is the tooth angle from the ξ–η axis (e.g. $\phi = [0, \pi/3, 2\pi/3, \pi, 4\pi/3, 5\pi/3]$, $\Delta\phi_i = \phi_i - \phi_{i-1} = \pi/3$ for a straight six-fluted symmetric tool), $\mathbf{T}(\Delta\phi_i)$ is found by substituting $\Delta\phi_i$ into Eq. (1), and τ_{0i} is the time between successive tooth passages where the indices are required for uneven tooth spacing. This angular notation is consistent with Metzler et al. [13]:

$$\tau_{0i} = \frac{\Delta\phi_i}{\Omega}. \tag{7}$$

The local cutting pressure, k_s, used in Eq. (6) was 2.84×10^8 N/m^2 [14] with a cutting direction angle, α, of 20° for zero rake angle [15] as shown in Fig. 4(b). The specific cutting pressure value is similar to previous values found for aluminum, where Al 6061-T6 equaled 2.06×10^8 N/m^2 [16], and Al 7075-T6 equaled 8.50×10^8 N/m^2 [17]. In this analysis, k_s is considered a constant that is independent of cutting speed. Stephenson and Agapiou [15] have shown that steady-state forces change with cutting conditions such as speed. However, these changes have minimal impact on magnitude and no impact on the frequency content of the stability predictions. Constant local cutting pressure has been used successfully in the past for predicting stability regions [3–5]. The final form of the cutting force for a symmetric tool using a constant time delay for each tooth, such that $\tau_{0i} = \tau_0$, and $\Delta\phi_i = \Delta\phi$ for all teeth is

$$\begin{bmatrix} F_{c\xi} \\ F_{c\eta} \end{bmatrix} = L_{\text{nom}}\mathbf{K}_{cc}(\mathbf{I}\vec{\xi}(t) - \mu\mathbf{T}(\Delta\phi)\vec{\xi}(t-\tau_0)), \tag{8}$$

$$\mathbf{K}_{cc} = \left(2\mu_r + \frac{1}{\tan\,\rho}\right)k_s \sum_{i=1}^{N_t} \begin{bmatrix} c_i C_i & s_i C_i \\ c_i S_i & s_i S_i \end{bmatrix}. \tag{9}$$

2.3. Process-damping forces

Vibrations of the cutting tool result in an uneven work surface, thus varying the effective tool clearance angle causes an additional radial (bending) force. As noted in Delio et al. [18], the additional force is 90° out of phase with the tool displacement, and increases with the spatial frequency of the surface variations. These observations lead to a first-order model of the process-damping phenomenon for turning, first suggested by Tobias [1], where r_0 is the tool radius, and μ_f is friction:

Normal force:

$$F_n \propto -\frac{\mathrm{d}r}{\mathrm{d}s} = -\frac{\mathrm{d}r}{\mathrm{d}t}\frac{\mathrm{d}t}{\mathrm{d}s} = -\dot{r}\,\frac{1}{\Omega r_0}, \tag{10}$$

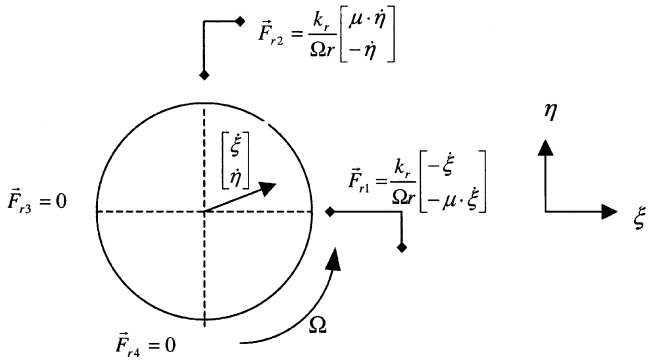

Fig. 6. Process damping for a four-fluted reamer Tool velocity is shown in the positive ξ–η direction, causing rubbing on tooth 1 and 2. Force vector equations shown for all teeth.

Frictional force:

$$F_t = \mu_f F_n. \tag{11}$$

Tool velocity from vibration causes a contact force to occur normal to the margin-wall interference, with friction providing an orthogonal component. The contact force is found by using a rubbing stiffness coefficient (k_r in N/rad) for small angles, which is dependent on material and margin geometry. Previous research in turning assumes process damping to be similar to indenting [16,19], which multiplies a material dependent variable by a displaced volume that depends on the tool nose radius and flank relief angle. The proportionality of tool velocity divided by rotational velocity is consistent for both the prior turning model and the reaming model in this paper (see also Fig. 6). However, due to the differences between turning and reaming tools, it would be unjustified to place the quantitative turning values into the reaming model. Since an experimental method to determine k_r for reaming has not been shown in past research, and is beyond the scope of this paper, a study using different values of k_r will be used to show the qualitative change in stability as the value increases. Using the following geometric equations for each cutting tooth, subscript i, a summation of the assumed rubbing forces on each tooth can be assembled into a lumped force in the ξ–η frame:

$$\dot{r}_i(t) = [c_i \; s_i]\begin{bmatrix}\dot{\xi}(t)\\ \dot{\eta}(t)\end{bmatrix}, \quad \begin{bmatrix}F_{r\xi}(t)\\ F_{r\eta}(t)\end{bmatrix} = \mathbf{C}_{pd}(\Omega)\begin{bmatrix}\dot{\xi}(t)\\ \dot{\eta}(t)\end{bmatrix}, \tag{12,13}$$

$$\begin{aligned}\mathbf{C}_{pd}(\Omega) &= \frac{k_r}{r_0\Omega}\frac{1}{2}\sum_{i=1}^{N_t}\begin{bmatrix}-c_i & s_i\\ -s_i & -c_i\end{bmatrix}\begin{bmatrix}1\\ \mu_f\end{bmatrix}[c_i \; s_i], \quad \text{general}\\ &= \frac{N_t}{4}\frac{k_r}{r_0\Omega}\begin{bmatrix}-1 & \mu_f\\ -\mu_f & -1\end{bmatrix}, \quad \text{symmetric reamer.}\end{aligned} \tag{14}$$

The complete process-damping matrix, $\mathbf{C}_{pd}$, accounts for a lumped value based on material, margin geometry, tool radius, tooth spacing, and spindle speed.

3. Stability analysis

The equations of motion in the ξ–η frame can be simplified into the form of an eigenvalue problem to solve for the stability limit. The eigenvalue corresponds to the value for L_{nom}; therefore, the eigenvalue must be a positive real value for the solution to have physical meaning:

$$\mathbf{M}_\xi \ddot{\vec{\xi}}(t) + \mathbf{C}_\xi \dot{\vec{\xi}}(t) + \mathbf{K}_\xi \vec{\xi}(t) = \begin{bmatrix} \vec{F}_\xi(t) \\ \vec{F}_\eta(t) \end{bmatrix}, \tag{15}$$

where

$$\mathbf{M}_\xi = (\mathbf{T}^{-1}(\vartheta)\mathbf{M}), \quad \mathbf{C}_\xi = (\mathbf{T}^{-1}(\vartheta)\mathbf{C}_r), \quad \mathbf{K}_\xi = (\mathbf{T}^{-1}(\vartheta)\mathbf{K}_r),$$

$$\begin{bmatrix} \vec{F}_\xi(t) \\ \vec{F}_\eta(t) \end{bmatrix} = L_{\text{nom}}\mathbf{K}_{cc}(\mathbf{I}\vec{\xi}(t) - \mu\mathbf{T}(\Delta\phi)\vec{\xi}(t-\tau_0)) + \mathbf{C}_{pd}\dot{\vec{\xi}}(t). \tag{16}$$

Since L_{nom} does not multiply $\mathbf{C}_{pd}$, it will be moved to the left-hand side of the equation. Combining Eqs. (15) and (16) gives the following equation of motion:

$$\mathbf{M}_\xi \ddot{\vec{\xi}}(t) + (\mathbf{C}_\xi - \mathbf{C}_{pd})\dot{\vec{\xi}}(t) + \mathbf{K}_\xi \vec{\xi}(t) = (L_{\text{nom}}\mathbf{K}_{cc}(\mathbf{I}\vec{\xi}(t) - \mu\mathbf{T}(\Delta\phi)\vec{\xi}(t-\tau_0))). \tag{17}$$

The desired result of the analysis is a set of parameters: spindle speed, frequency of vibration, and radial depth of cut $\{\Omega, \omega, L_{\text{nom}}\}$, which satisfies the equations of motion at the limit of stability, given all other parameters in the equations of motion. At the limit of stability the tool motion will be periodic, allowing the desired values to be obtained by satisfying the Laplace transform of the equations of motion where $s = \mathrm{i}\omega$:

$$(\mathbf{I} - L_{\text{nom}}\mathbf{G}_{pd}(\omega,\Omega)\mathbf{R}(\omega,\Omega))\begin{bmatrix} \bar{\xi} \\ \bar{\eta} \end{bmatrix} = \begin{bmatrix} 0 \\ 0 \end{bmatrix}, \tag{18}$$

where

$$\mathbf{G}_{pd}(\omega,\Omega) = [-\omega^2\mathbf{M}_\xi + \mathrm{i}\omega(\mathbf{C}_\xi - \mathbf{C}_{pd}) + \mathbf{K}_\xi]^{-1},$$

$$\mathbf{R}(\omega,\Omega) = \mathbf{K}_{cc}(\mathbf{I} - \mu\mathrm{e}^{-\mathrm{i}\omega\tau_0}\mathbf{T}(\Delta\phi)).$$

Note in the regeneration matrix, $\mathbf{R}$, if μ is equal to or greater than 1, a trivial solution can be found without regard to the stability value, L_{nom}, which is why μ, Eq. (5), must always be less than one. An eigenvalue problem is now formed for the matrix $\mathbf{P}_{pd}$ where L_{nom} is the solution to a given chatter frequency (ω) and spindle speed (Ω). Since the eigenvalue is complex, but L_{nom} is a physical value that must be positive, the usable solutions only occur when the imaginary part is equal to zero, and the real part is positive:

$$(\mathbf{I} - L_{\text{nom}}\mathbf{P}_{pd}(\omega,\Omega))\begin{bmatrix} \bar{\xi} \\ \bar{\eta} \end{bmatrix} = \begin{bmatrix} 0 \\ 0 \end{bmatrix}, \tag{19}$$

where

$$\mathbf{P}_{pd}(\omega, \Omega) = \mathbf{G}_{pd}(\omega, \Omega)\mathbf{R}(\omega, \Omega).$$

4. Solution method

The solution to the matrix problem in Eq. (19) has two complex eigenvalues that will be sorted in ascending order so the first eigenvalue always has the smallest absolute value. Since this is a linear system, the eigenvalue provides information on whether the system is stable, critically stable, or unstable. The following numbered steps outline the numerical method to find the eigenvalue solutions that are real and positive: (1) set spindle speed, Ω, and define the tool dynamic matrices; (2) solve the eigenvalue problem for a range of frequencies, ω, with resolution $\Delta\omega$; (3) sort the eigenvalues into ascending order so the first eigenvalue always has the smallest absolute value; (4) check if the imaginary part of each eigenvalue crosses the zero axis (this occurs when the sign of the imaginary part changes in the interval $\Delta\omega$); (5) a numerical search is then used to find a more precise solution (a two-point method (regula-falsi) was chosen because it encapsulates the solution; an iteration stop must be used because a sign change can occur at a singularity where no root is present); (6) if a zero-axis crossing of the imaginary term is found, then check if the real part of the root is greater than zero; if so, save the real part, which is equal to L_{nom}, in addition, save the values Ω and ω that produced this usable solution; (7) repeat for a range of spindle speeds.

The output for each iteration with a usable solution is the set $\{\Omega, \omega, L_{\text{nom}}\}$, which defines the borders of stability.

5. Numerical simulation

Results from an Euler simulation will be used for comparison with the analytical results. The simulation uses Euler integration of Eq. (17) to produce results such as stability, frequencies, and hole form. The simulation should match the stability predictions. For comparison to the analytical solution, nine revolutions were run. The stability criterion was determined by comparing the maximum radius during the last two revolutions with the maximum radius of the previous two revolutions and the change in the mean radius over the same interval. Since this is a linear model, an unstable solution moves toward infinity, while a stable solution moves toward zero. For this reason, the output often has small numbers because the more the revolutions run in the simulation, the closer the value moves toward zero, but qualitatively it shows the basic hole form found in the experiment.

All of the forces acting on the tool modal mass must be found to determine tool motion. These forces include the cutting and process damping, and the stiffness and damping in the structure. The subscript, n, denotes the time step, dt, since the equation must be converted to a discrete form. The number of steps for the time delay is denoted by the subscript τ:

$$\vec{F}_{\text{tot},n} = -\mathbf{C}_{\xi}\dot{\vec{\xi}}_n - \mathbf{K}_{\xi}\vec{\xi}_n + (L_{\text{nom}}\mathbf{K}_{cc}(\mathbf{I}\vec{\xi}_n - \mu\mathbf{T}(\Delta\phi)\vec{\xi}_{n-\tau})) + \mathbf{C}_{pd}\dot{\vec{\xi}}_n. \tag{20}$$

Once the forces were found, the acceleration of the tool point mass was determined using Newton's second law

$$\ddot{\vec{\xi}}_{n+1} = (\mathbf{M}_{\xi})^{-1}\vec{F}_{\mathrm{tot},n}. \tag{21}$$

Using kinematic approximations, velocity and displacement were determined for the tool at the next time step:

$$\dot{\vec{\xi}}_{n+1} = \dot{\vec{\xi}}_{n} + \mathrm{d}t\,\ddot{\vec{\xi}}_{n+1}, \quad \vec{\xi}_{n+1} = \vec{\xi}_{n} + \mathrm{d}t\,\dot{\vec{\xi}}_{n+1}. \tag{22,23}$$

The smaller the time step used, the less the error, but the slower the computational time. In addition, when the time step became too large, numerical instability occurred. The time step chosen to prevent this instability was 1/300 of the smaller number between the tool natural period and the period of rotation. Convergence was checked at each spindle speed.

The validation of this simulation technique to the analytical solution is important in future work that may include nonlinear forcing functions, irregular spaced cutting teeth, or an initial

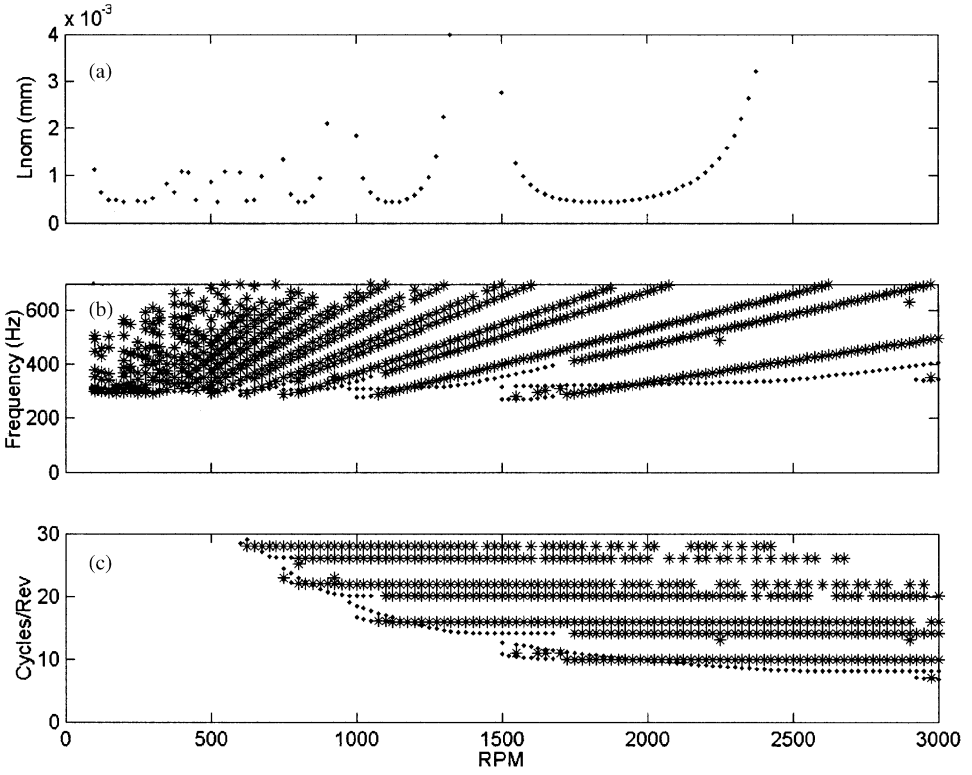

Fig. 7. Stability boundaries for a six-flute reamer with no process damping. Tool dynamics are identical in both Ξ–H directions: $\omega_n = 292\,\mathrm{Hz}$, $k = 186{,}000\,\mathrm{N/m}$, $\zeta = 0.002$. Cutting process parameters: $k_r = 0\,\mathrm{N/rad}$, $\mu = 0.94$, $k_s = 2.84 \times 10^8\,\mathrm{N/m^2}$. Dots are solutions for 1st, and stars are solutions for 2nd eigenvalue. (a) L_{nom}, (b) frequency, (c) cycles per revolution.

hole profile that cannot be solved analytically. In addition, the numerical simulation produces hole-form results.

6. Results

Machining stability boundaries are often plotted with rpm and DOC (L_{nom}), parameters that are conveniently controlled by the machine tool operator. The following subsections show the model's predicted stability boundaries using previous models and with velocity-dependent process-damping forces added to the external force model.

6.1. Cutting forces only

The stability boundary has a repetitive u-like structure, as shown in Fig. 7. Each point represents a neutrally stable analytical solution. Parameter combinations above the boundary are unstable. Each region has infinite L_{nom} at the natural frequency, a minimum value at a slightly higher frequency, and a progression back toward infinite L_{nom} as the frequency approaches infinity. Overlap of neighboring regions keeps stable L_{nom} values

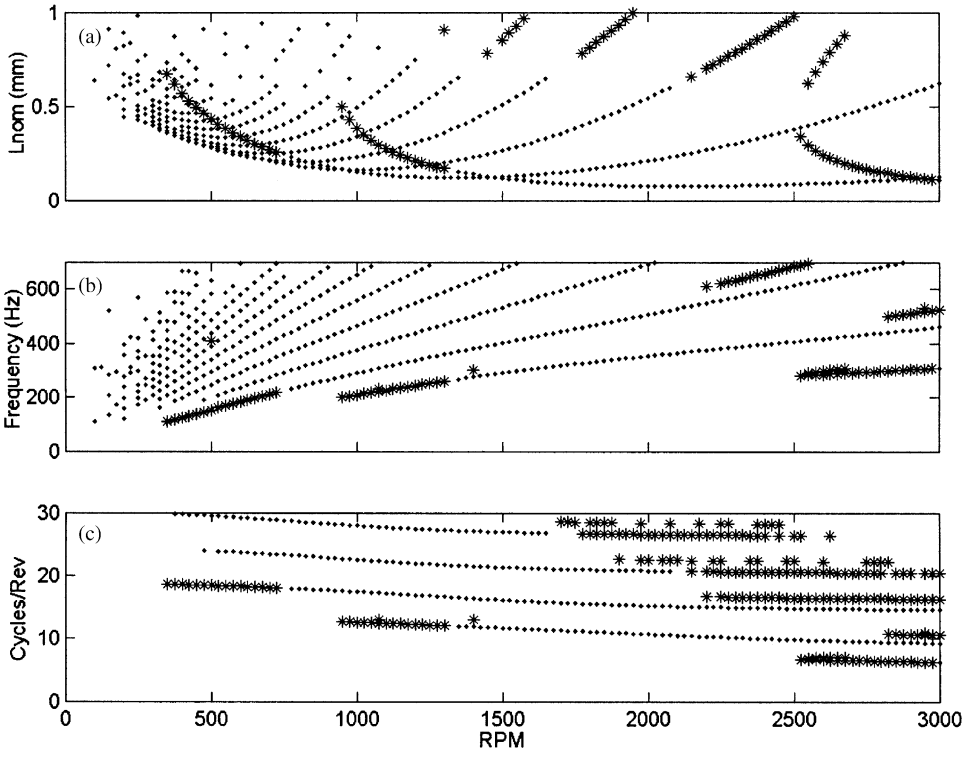

Fig. 8. Stability boundaries for a six-flute reamer with process damping: $k_r = 50\,\mathrm{N/rad}$, $\mu_f = 0.25$. Dots are solutions for 1st, and stars are solutions for 2nd eigenvalue. (a)–(c) as in Fig. 7.

finite. Since the regeneration factor, μ, is less than one, there are unique lobes and chatter frequencies at most values of Ω. The unstable frequencies are then mapped into Fig. 7(b), where they all occur above the tool natural frequency. Fig. 7(c) normalizes the left axis to tool cycles per spindle revolution.

6.2. Inclusion of process-damping forces

In Fig. 8 a low value of process damping causes the low limit to increase, and higher values of L_{nom} can be obtained at lower cutting speeds. This is similar to the effect in 1 dof system [16,18,19]. Process damping is inversely proportional to spindle speed, so stability generally increases for decreasing spindle speeds.

As levels of process damping are increased in Fig. 9, additional solutions are obtained for frequencies of vibration below the tool natural frequency. The first eigenvalue is plotted with a dot, and the second eigenvalue is plotted with a star. The shape of the solution set changes significantly as process damping is added, and the value of L_{nom} increases significantly as process damping is increased. The numerical simulation output for a four-flute reamer is compared to the analytical solution in Fig. 10, where the $*$ are stable and 0 are

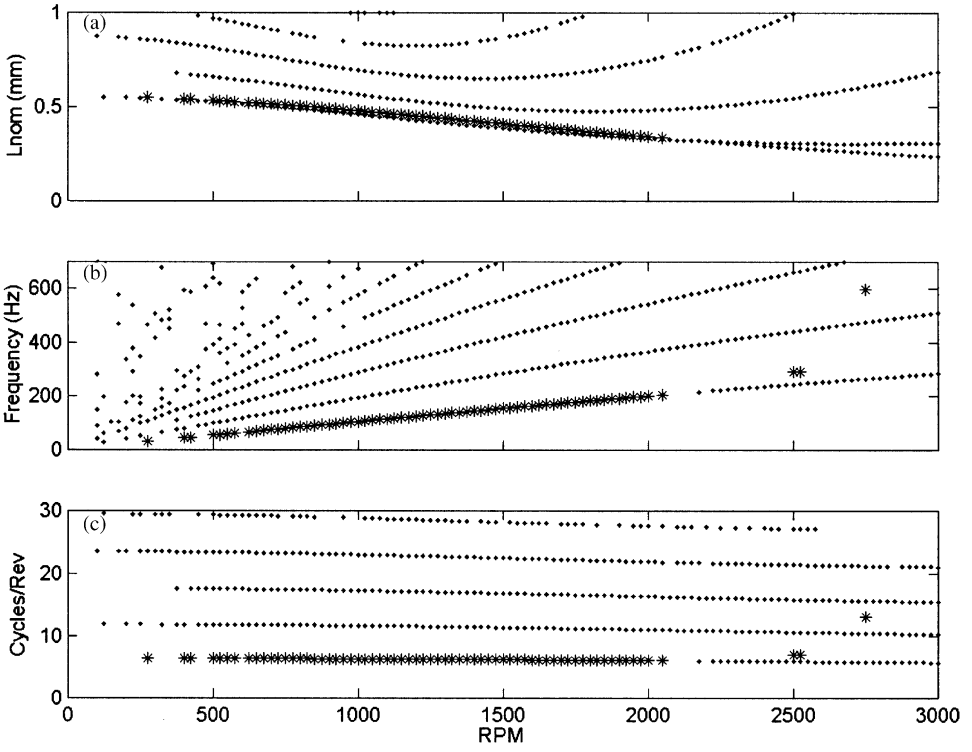

Fig. 9. Stability boundaries for a six-flute reamer with process damping: $k_r = 200\,\text{N/rad}$, $\mu_f = 0.25$. Dots are solutions for 1st, and stars are solutions for 2nd eigenvalue. (a)–(c) as in Fig. 7.

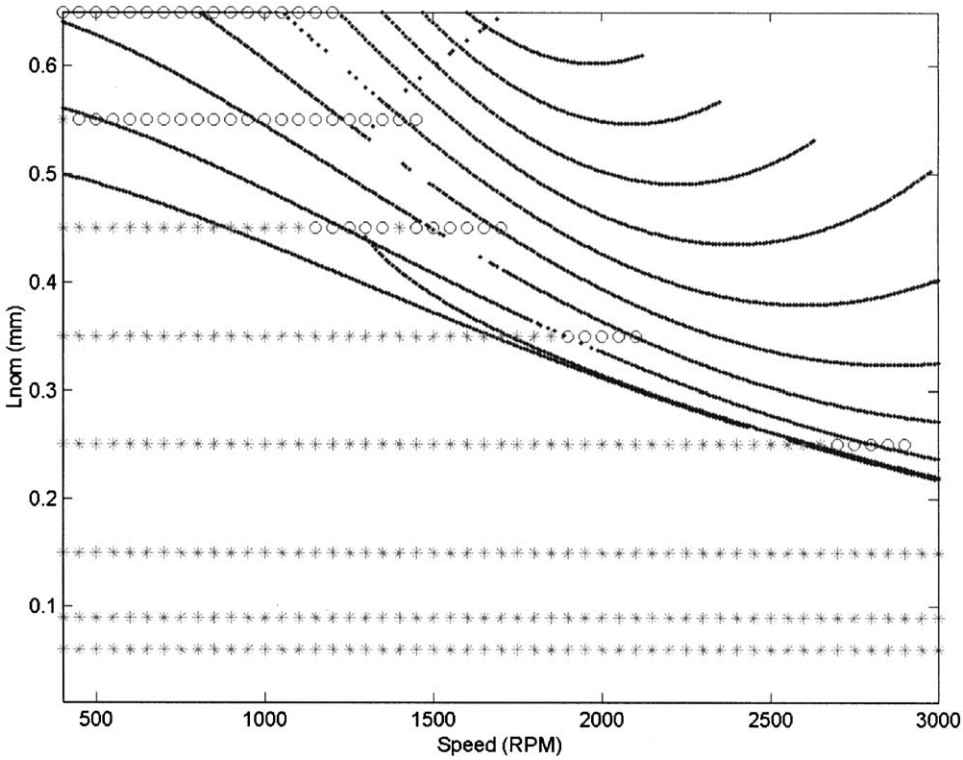

Fig. 10. Stability boundaries obtained by frequency domain analysis (dots) for a four-flute reamer. Simulation data shown by stars (stable) and circles (unstable). Stability boundaries for a four-flute reamer with process damping, $k_r = 80\,\mathrm{N/rad}$. Tool dynamics are identical in both Ξ–H directions: $\omega_n = 382\,\mathrm{Hz}$, $k = 52,400\,\mathrm{N/m}$, $\zeta = 0.006$. Cutting process parameters: $k_r = 0\,\mathrm{N/rad}$, $\mu = 0.83$, $\mu_f = 0.5$, $k_s = 2.84 \times 10^8\,\mathrm{N/m^2}$.

unstable solutions from simulation. The numerical simulation matches well with the analytical solution.

The hole form for a six-fluted reamer from the simulation is shown in Figs. 11 and 12. A three-dimensional plot of a single spindle revolution is shown in Fig. 11. It can be seen that the form helically moves down the hole, so the motion is not at an exact integer multiple of spindle speed. A cross-section of the hole is shown in Fig. 12, which shows the profile that would be found by gauging the hole. Similar plots are shown in Fig. 13 for a four-fluted reamer. It can be seen that with enough process damping, the four-fluted reamer generates a five-lobed hole and the six-fluted reamer generates a seven-lobed hole. Therefore, as process damping increases, several phenomena are observed.

- The minimum value (L_{nom}) increases with increasing levels of process damping.
- Secondary unstable solutions with frequency less than the natural frequency become available as process damping is increased. These solutions eventually become dominant as process damping increases.

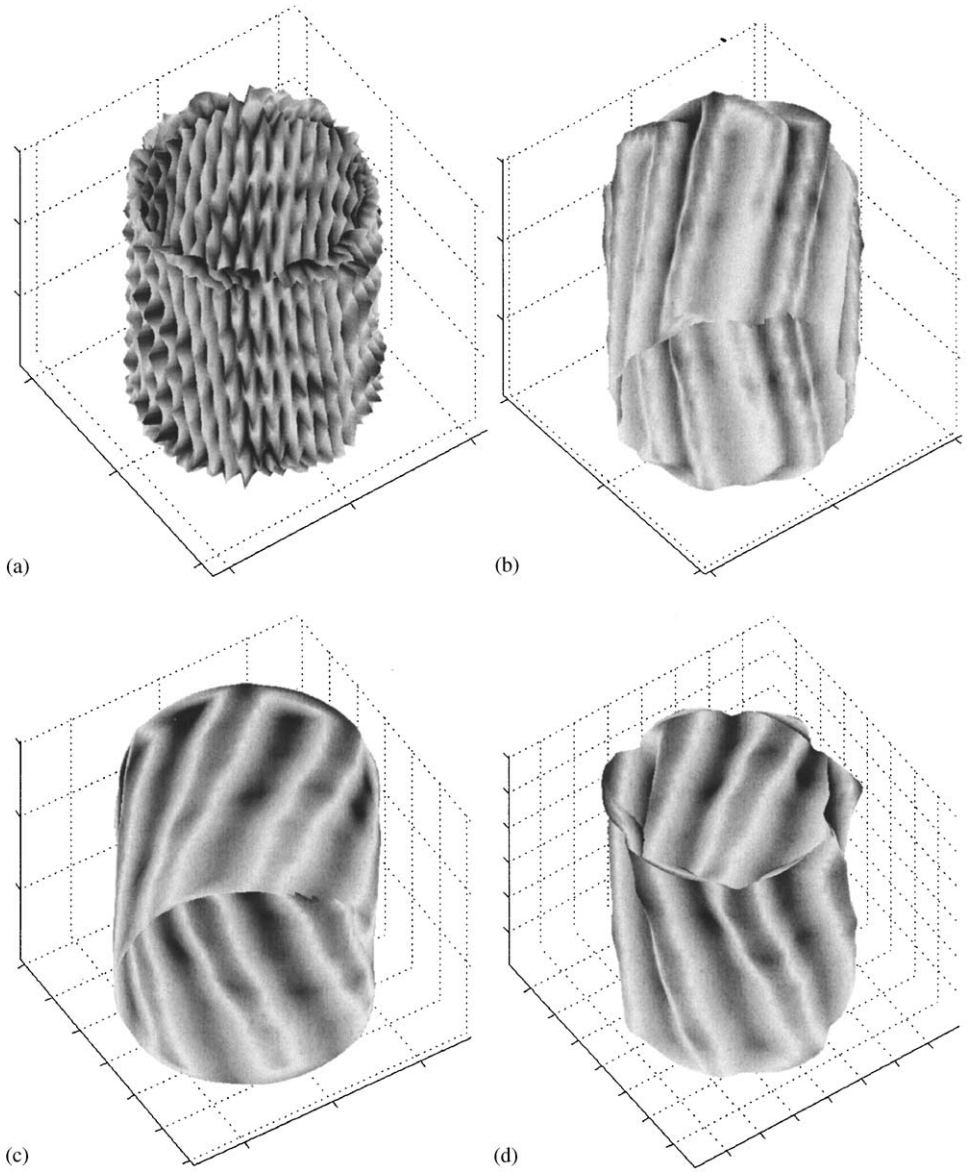

Fig. 11. Three-dimensional plot of the hole for one revolution of a six-flute reamer. Tool dynamics are identical in both Ξ–H directions: $\omega_n = 292\,\text{Hz}$, $k = 186,000\,\text{N/m}$, $\zeta = 0.002$. Cutting process parameters: $\mu = 0.94$, $k_s = 2.84 \times 10^8\,\text{N/m}^2$, $\mu_f = 0.25$. (a) $k_r = 50\,\text{N/rad}$, feed $= 0.15\,\text{mm/rev}$; (b) $k_r = 100\,\text{N/rad}$, feed $= 0.15\,\text{mm/rev}$; (c) $k_r = 200\,\text{N/rad}$, feed $= 0.15\,\text{mm/rev}$; (d) $k_r = 200\,\text{N/rad}$, feed $= 0.30\,\text{mm/rev}$.

- The approximate lower frequency $MN_t + 1$ ($N_t =$ number of teeth, $M =$ arbitrary integer) cycles per revolution are found as process damping is increased, which are usually seen in practice.
- When process damping reaches a given level, the stability region practically loses dependence on spindle speed.

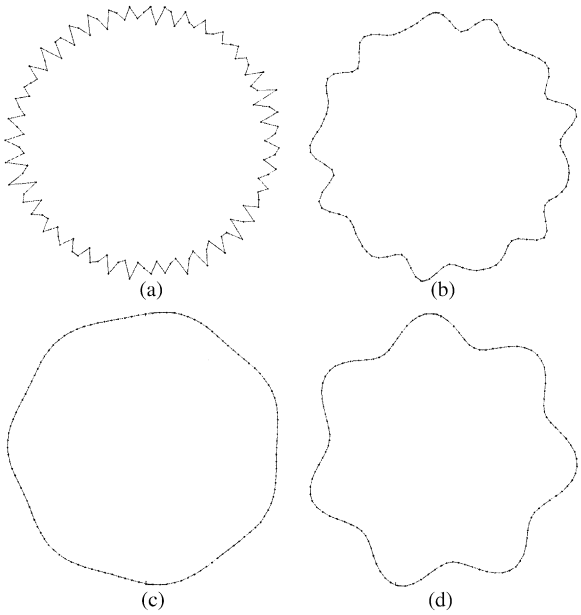

Fig. 12. Cross-sections of the hole from Fig. 1, respectively.

7. Summary and conclusion

A dynamic model of reaming, which includes a process-damping model similar to that used in turning and milling, is studied analytically. A stability analysis of the equations of motion leads to an eigenvalue problem that yields a combination of frequency, spindle speed, and depth of cut that produces borderline stable processes.

Hole form is shown to be dependent on the dynamics of the cutting process. The inclusion of a simple process-damping model leads to the prediction of low-frequency modes which appear to correspond to hole-form errors commonly found in practice.

The assumption that process damping eliminates chatter may be true, but low-frequency unstable solutions arise as process damping is added, leading to hole-form error. The current model is derived using kinetics, thus having predictive qualities. It shows a qualitatively accurate result, and it explains a mechanism consistent with long-standing observations and qualitative experimental data. The quantitative accuracy is not specified, since the process damping parameter of the reamer is unknown as it moves through the hole. It is also true that the effective tool stiffness increases as the tool moves through the hole [20], which is not modeled in this paper. The increased stiffness will affect the tool's natural frequency, but it should not affect the low-frequency vibration modeled in this paper.

Experimental studies are necessary to improve the accuracy of the process-damping model presented in this paper. This model was built from quantitative structural and cutting force models, while the process-damping values were varied over a large range. The results from the model reproduce experimentally observed phenomenon of low-frequency vibration.

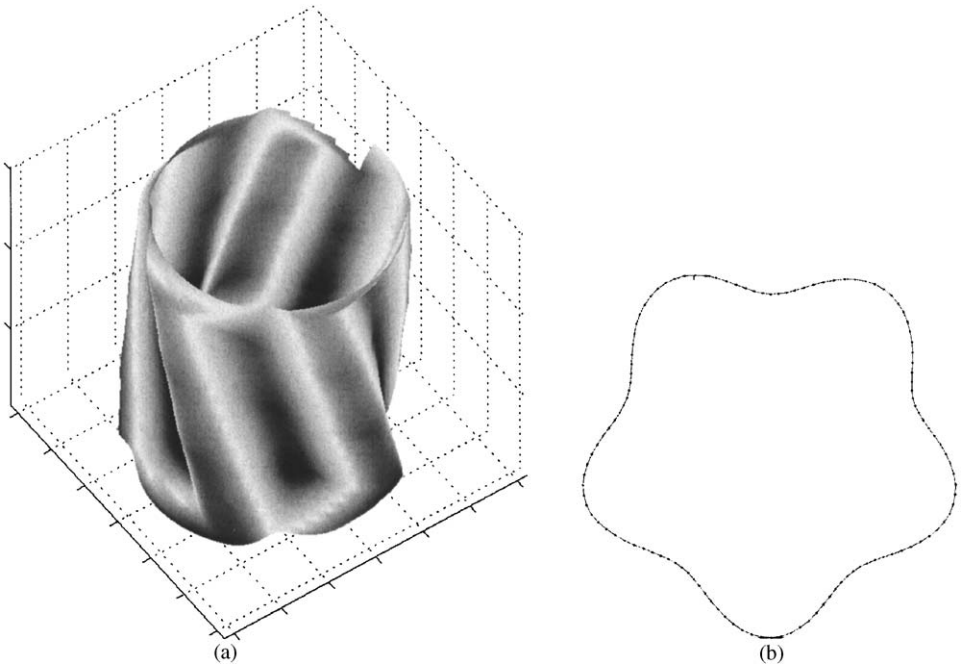

Fig. 13. Four-flute reamer with $\omega_n = 382\,\text{Hz}$, $k = 52,400\,\text{N/m}$, $\zeta = 0.006$. Cutting process parameters: $k_r = 300\,\text{N/rad}$, $\mu_f = 0.25$, $k_s = 2.84 \times 10^8\,\text{N/m}^2$. (a) Three-dimensional plot of the hole for one revolution, (b) cross-section of hole.

Acknowledgements

This research was supported by the Boeing Company and the National Science Foundation Grants CMS #9625161 & DMII #9900108.

References

[1] S.A. Tobias, *Machine Tool Vibration*, Blackie and Son, Bishopbriggs, UK, 1965.
[2] F. Koenigsberger, J. Tlusty, *Structures of Machine Tools*, Pergamon Press, Oxford, 1970.
[3] J. Tlusty, Machine dynamics, in: R.I. King (Ed.), *Handbook of High Speed Machining Technology*, Chapman & Hall, New York, 1985.
[4] I. Minis, R. Yanushevsky, A new theoretical approach for the prediction of machine tool chatter in milling, *Journal of Engineering for Industry* 115 (1993) 1–8.
[5] Y. Altintas, E. Budak, Analytical prediction of stability lobes in milling, *Annals of the CIRP* 44 (1) (1995) 357–362.
[6] H. Fujii, E. Marui, S. Ema, Whirling vibration in drilling—part I: cause of vibration and role of chisel edge, *Journal of Engineering for Industry* 108 (1986) 157–162.
[7] H. Fujii, E. Marui, S. Ema, Whirling vibration in drilling—part II: influence of drill geometries, particularly of the drill flank, on the initiation of vibration, *Journal of Engineering for Industry* 108 (1986) 163–168.
[8] H. Fujii, E. Marui, S. Ema, Whirling vibration in drilling—part III: vibration analysis in drilling workpiece with pilot hole, *Journal of Engineering for Industry* 110 (1988) 315–321.

[9] K. Sakuma, H. Kiyota, Hole accuracy with carbide-tipped reamers: 1st report, *Bulletin of the Japan Society of Precision Engineering* 19 (1986) 89–95.
[10] K. Sakuma, H. Kiyota, Behavior of tool and its effect on sectional profile of hole in reaming, *Memoirs of the Faculty of Engineering, Kyushu University* 42 (1982) 335–354.
[11] C.J. Li, A.G. Ulsoy, W.J. Endres, The effect of tool rotation on regenerative chatter in line boring, in: R.P.S. Han, K.H. Lee, A.C.J. Luo (Eds.), *Dynamics, Acoustics and Simulations*, ASME Publication DE 98, 1998, pp. 235–243.
[12] P.V. Bayly, K.A. Young, S.G. Calvert, J.E. Halley, Analysis of tool oscillation and hole roundness error in quasi-static model of reaming, *Journal of Manufacturing Science and Engineering* 123 (2001) 387–396.
[13] S.A. Metzler, P.V. Bayly, K.A. Young, J.E. Halley, Analysis and simulation of radial chatter in drilling and reaming, in: *Proceedings of DETC99: 1999 ASME Design Engineering Technical Conference*, 1999.
[14] B.T. Whitehead, The Effect of Process Damping on Stability and Hole Form in Drilling, Masters Thesis, Washington University, St. Louis, 2001.
[15] D.A. Stephenson, J.S. Agapiou, *Metal Cutting: Theory and Practice*, Marcel Dekker, New York, 1996.
[16] R.Y. Chiou, S.Y. Liang, Chatter stability of a slender cutting tool in turning with tool wear effects, *International Journal of Machine Tools and Manufacture* 38 (1998) 315–327.
[17] J. Tlusty, *Manufacturing Processes and Equipment*, Prentice-Hall, Englewood Cliffs, NJ, 2000.
[18] T. Delio, S. Smith, J. Tlusty, C. Zamudio, Stiffness, stability, and loss of process damping in high speed machining, ASME Publication PED, *Fundamental Issues in Machining* 43 (1990) 171–191.
[19] B.E. Clancy, Y.C. Shin, A comprehensive chatter predication model for face turning operation including the tool wear effect, *International Journal of Machine Tools and Manufacture* 42 (2002) 1035–1044.
[20] D.N. Dilley, Accuracy, Vibration, and Stability in Drilling and Reaming, DSc Dissertation, Washington University, St. Louis, 2003.